Asymmetric Bimanual Control of Dual-Arm Exoskeletons for Human-Cooperative Manipulations

Zhijun Li, *Senior Member, IEEE*, Bo Huang, Arash Ajoudani, Chenguang Yang, *Senior Member, IEEE*, Chun-Yi Su, *Senior Member, IEEE*, and Antonio Bicchi, *Fellow, IEEE*

***Abstract*—In this paper, two upper limbs of an exoskeleton robot are operated within a constrained region of the operational space with unidentified intention of the human operator's motion as well as uncertain dynamics including physical limits. The new human-cooperative strategies are developed to detect the human subject's movement efforts in order to make the robot behavior flexible and adaptive. The motion intention extracted from the measurement of the subject's muscular effort in terms of the applied forces/torques can be represented to derive the reference trajectory of his/her limb using a viable impedance model. Then, adaptive online estimation for impedance parameters is employed to deal with the nonlinear and variable stiffness property of the limb model. In order for the robot to follow a specific impedance target, we integrate the motion intention estimation into a barrier Lyapunov function based adaptive impedance control. Experiments have been carried out to verify the effectiveness of the proposed dual-arm coordination control scheme, in terms of desired motion and force tracking.**

***Index Terms*—Barrier Lyapunov function (BLF), dual-arm exoskeletons, human-cooperative manipulations, variable stiffness.**

I. Introduction

In the past decades, exoskeleton robots have been developed for human power augmentation and rehabilitation training [1]. One of the most critical issues in controlling a robotic exoskeleton is to enable the robots to understand the human's motion intention so that the robots could actively cooperate with the human subject. According to [1], the bimanual tasks for dual-arm manipulation can be classified into two categories: symmetric bimanual task and asymmetric bimanual task. In practice, most tasks need bimanual dual-arm cooperation in an asymmetric manner, and asymmetric tasks bring more challenges in the control design than symmetric tasks do. In this paper, we develop an asymmetric bimanual coordination control for a dual-arm exoskeleton system to cooperate with a human in which the left hand is holding a canvas whereas the right hand a pen drawing a line by tracing a circular trajectory on the canvas. In [2] and [3], the velocities of the two manipulators' end-effectors can be viewed as relative motions by the introduction of a relative Jacobian, which combines the individual Jacobians of both manipulators together. In [4], by using the relative Jacobian, the kinematic redundancy of the dual-arm system was utilized for optimizing torque distributions. In [5], both kinematics and dynamics using the relative Jacobian were presented, and the robust/model-free impedance controller for a dual-arm system was proposed. However, the aforementioned works focus on industrial manipulators without consideration of human participation. Moreover, each manipulator is assumed to be redundant and far from singular configurations, while in practice, singularities and physical constraints can be encountered during the performance of the task. Thus, it is necessary to investigate cooperative control strategies into the task requirements and handle the various constraints at the same time.

In human–robot cooperative manipulation, to enable a robot to actively collaborate with the human operator, we must solve the problem of how to make the exoskeleton robot understand the motion intention of the human operator. In the robotics community, impedance control has been regarded as an effective approach to achieve the physical human–robot interaction. When a human subject intends to change the motion, a load force would be produced as the robot extracts its motion in terms of the force exerted by the human subject. To solve this problem, we expect to estimate the motion intention of the human operator and integrate it into the control system design. In this paper, we use the position and force sensors as a communication medium between human arms and robot arms. In order to estimate the motion intention of the human operator from available sensory information, many efforts have been made [6], [7]. However, one of the main problems of these works is that the variable stiffness property was not considered in the impedance model for motion intention estimation. Consequently, the estimation may not be accurate enough.

On the other hand, special consideration should also be taken into account for the dual-arm exoskeleton with position and velocity constraints in manipulation tasks for avoiding the singularity region, physical limits, dangerous region, etc. It is necessary to carefully deal with the constraints in the control design. For robot control design, barrier Lyapunov functions (BLF) emerge as a promising approach for handling such physical constraints such as joint limits, torque limits, and safety zones [8], [9]. Considering the problems mentioned above, in this paper, we propose an asymmetric bimanual coordinate control for the dual-arm exoskeleton to perform human-cooperative manipulation. The contributions can be summarized as follows.

Manuscript received June 1, 2016; revised September 12, 2016, March 7, 2017, and July 13, 2017. Date of publication November 10, 2017; date of current version February 5, 2018. This paper was recommended for publication by Associate Editor R. D. Gregg and Editor A. Kheddar upon evaluation of the reviewers' comments. This work was supported in part by the National Natural Science Foundation of China under Grant 61573147, Grant 91520201, and Grant 61625303, in part by the Guangzhou Research Collaborative Innovation Projects under Grant 2014Y2-00507, in part by the Guangdong Science and Technology Research Collaborative Innovation Projects under Grant 2014B090901056 and Grant 2015B020214003, and in part by the Guangdong Science and Technology Plan Project (Application Technology Research Foundation) under Grant 2015B020233006. *(Corresponding author: Chenguang Yang.)*

Z. Li is with the Department of Automation, University of Science and Technology of China, Hefei 230000, China, and also with the College of Automation Science and Engineering, South China University of Technology, Guangzhou 510630, China (e-mail: zjli@ieee.org).

B. Huang and C. Yang are with the College of Automation Science and Engineering, South China University of Technology, Guangzhou 510630, China (e-mail: huangbo_2015@163.com; cyang@ieee.org).

A. Ajoudani and A. Bicchi are with the Department of Advanced Robotics, Istituto Italiano di Tecnologia, Genova 16163, Italy, and also with the Interdepartmental Research Center "E. Piaggio," Faculty of Engineering, University of Pisa 56126, Italy (e-mail: arash.ajoudani@iit.it; bicchi@centropiaggio.unipi.it).

C.-Y. Su is with the Department of Mechanical, Industrial and Aerospace Engineering, Concordia University, Montreal QC H3G 1M8, Canada (e-mail: cysu@alcor.concordia.ca).

Color versions of one or more of the figures in this paper are available online at http://ieeexplore.ieee.org.

Digital Object Identifier 10.1109/TRO.2017.2765334

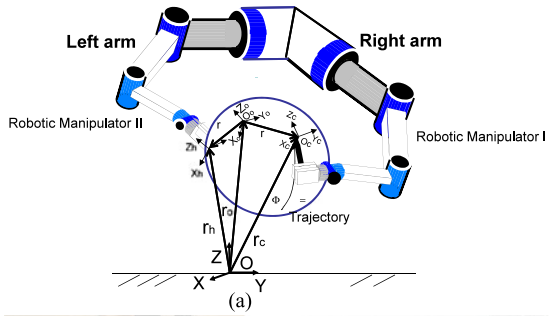

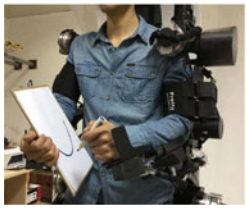

(b)

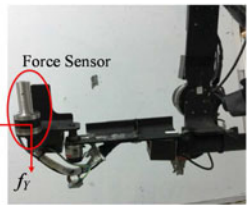

(c)

Fig. 1. (a) Schematic diagram of a dual arm. (b) Asymmetric bimanual tasks. (c) Location of force sensor.

1) The force caused by the subject's muscular effort that is reflected during the interaction is used to detect the intention of the human operator's motion.
2) The approach of impedance parameters approximation is presented to estimate the variable stiffness, with the instantaneous measurements of the force and the position of the dual-arm end-effectors.
3) A novel BLF-based adaptive impedance control is proposed for the dual-arm exoskeleton in consideration of the position and velocity constraints.

II. System Description

The illustration of asymmetric bimanual manipulation by our dual-arm robot is shown in Fig. 1(a), where the manipulator II's end-effector tightly holds the circular object moving as required in the task space, and the manipulator I's end-effector follows a desired trajectory on the circular object while imposing a given certain force on the circular object, where $O_oX_oY_oZ_o$ is the coordinate attached to the circular object and its origin is the mass center O_o; $O_hX_hY_hZ_h$ and $O_cX_cY_cZ_c$ are the coordinates on the manipulator II's end-effector and its origin is the mass center O_h, and the manipulator I's end-effector and its origin is the mass center O_c, respectively; and $OXYZ$ is the world coordinate.

The relative position of the system can be described by $\chi_c = \chi_o + A_o(\theta_o)\chi_{co}$, $\chi_h = \chi_o + A_o(\theta_o)\chi_{ho}$, $A_c = A_o(\theta_o)A_{co}(\theta_{co})$, $A_h = A_o(\theta_o)$, where $A_o(\theta_o) \in \mathbb{R}^{3\times3}$ represents the rotation matrix with regard to θ_o and $A_{co}(\theta_{co}) \in \mathbb{R}^{3\times3}$ denotes the rotation matrix with regard to θ_{co}; $A_c \in \mathbb{R}^{3\times3}$, χ_c, χ_h, and χ_o are the position vectors in $O_cX_cY_cZ_c$, $O_hX_hY_hZ_h$, and $O_oX_oY_oZ_o$, respectively, and χ_{co} is the position vector in $O_cX_cY_cZ_c$ expressed in $O_oX_oY_oZ_o$; χ_{ho} is the position vector in $O_hX_hY_hZ_h$ expressed in $O_oX_oY_oZ_o$; θ_c is the orientation vector of $O_cX_cY_cZ_c$; θ_o is the orientation vector of $O_oX_oY_oZ_o$; θ_{co} is the orientation vector of $O_cX_cY_cZ_c$ expressed in $O_oX_oY_oZ_o$; θ_{ho} is the orientation vector of $O_hX_hY_hZ_h$ expressed in $O_oX_oY_oZ_o$; $r_c = [\chi_c^T, \theta_c^T]^T \in \mathbb{R}^6$, $r_h = [\chi_h^T, \theta_h^T]^T \in \mathbb{R}^6$, $r_o = [\chi_o^T, \theta_o^T]^T \in \mathbb{R}^6$, $r_{co} = [\chi_{co}^T, \theta_{co}^T]^T \in \mathbb{R}^6$, $r_{ho} = [\chi_{ho}^T, \theta_{ho}^T]^T \in \mathbb{R}^6$. $\Phi(r_{co}) = 0$ is a trajectory drawn on the circular object expressed in $O_oX_oY_oZ_o$. Considering that the circular object is tightly grasped by the manipulator II, we have $\dot{r}_{ho} = [\dot{\chi}_{ho}^T, \dot{\theta}_{ho}^T]^T = 0$, accordingly, $\dot{\chi}_{ho} = 0$ and $\dot{\theta}_{ho} = 0$, then we can obtain the derivatives of the relative position as $\dot{\chi}_c = \dot{\chi}_o + A_o(\theta_o)\dot{\chi}_{co} - S(A_o(\theta_o)\chi_{co})\dot{\theta}_o$, $\dot{\chi}_h = \dot{\chi}_o - S(A_o(\theta_o)\chi_{ho})\dot{\theta}_o$, $\dot{\theta}_c = \dot{\theta}_o + A_o(\theta_o)\dot{\theta}_{co}$, $\dot{\theta}_h = \dot{\theta}_o$, where $S(t) = [0, -t_3, t_2; t_3, 0, -t_1; -t_2, t_1, 0]$ [2] with a given vector $t = [t_1, t_2, t_3]^T$. Define $\dot{X}_c = [\dot{\chi}_c^T, \dot{\theta}_c^T]^T$, $\dot{X}_o = [\dot{\chi}_o^T, \dot{\theta}_o^T]^T$, $\dot{X}_h = [\dot{\chi}_h^T, \dot{\theta}_h^T]^T$, and $\dot{X}_{co} = [\dot{\chi}_{co}^T, \dot{\theta}_{co}^T]^T$, we have the following relationship:

$$\dot{X}_{co} = R_A^{-1}\dot{X}_c - R_A^{-1}P\dot{X}_o \tag{1}$$

$$\dot{X}_h = Q\dot{X}_o \tag{2}$$

where $R_A = \mathrm{diag}[A_o(\theta_o), A_o(\theta_o)]$, $P = [I^{3\times3}, -S(A_o(\theta_o)\chi_{co}); 0, I^{3\times3}]$, $Q = [I^{3\times3}, -S(A_o(\theta_o)\chi_{ho}); 0, I^{3\times3}]$. Due to the rotation matrix $A_o(\theta_o)$, $A_o(\theta_o)A_o^T(\theta_o) = I^{3\times3}$ and $R_AR_A^T = I^{6\times6}$, it is obvious that $P \in \mathbb{R}^{6\times6}$ and Q are of full rank. From (1), one can obtain $\dot{X}_{co} = [R_A^{-1}, -R_A^{-1}P][\dot{X}_c^T, \dot{X}_o^T]^T$. Let $q = [q_A^T, q_B^T]^T \in \mathbb{R}^n$ be the dual-arm system's joint variables, $q_A \in \mathbb{R}^{n_A}$ and $q_B \in \mathbb{R}^{n_B}$ are the vectors of the manipulator I's and II's joint variables, respectively, and $n = n_A + n_B$ is the number of DOF of the dual-arm exoskeleton robot; n_A and n_B are number of DOF of the manipulators I and II, respectively. Considering $\dot{X}_c = J_A\dot{q}_A$ with $J_A \in \mathbb{R}^{6\times n_A}$ and $\dot{X}_o = J_B\dot{q}_B$ with $J_B \in \mathbb{R}^{6\times n_B}$, we have $\dot{X}_{co} = [R_A^{-1}, -R_A^{-1}P][J_A\dot{q}_A, J_B\dot{q}_B]^T = [R_A^{-1}J_A, -R_A^{-1}PJ_B]\dot{q}^T$, where $J_R = [R_A^{-1}J_A, -R_A^{-1}PJ_B] \in \mathbb{R}^{6\times n}$ is the relative Jacobian in the world coordination.

III. Human–Robot Cooperative Motion Generation

Various approaches have been proposed for estimating the stiffness of robot actuators [13]–[16]. However, these approaches cannot be applied to human–robot cooperation due to ignoring the estimation of human intention. In general, human intention can be represented by the applied force/torque to derive the system's reference motion, that is, it is passed to the system dynamics to determine the reference states of the system (velocity and position) through the human limb dynamic model [19], [20]. However, the muscle impedance of human limbs has been proven to be a mechanical transducer unit that can be possibly regulated during manipulation tasks and that demonstrates variable stiffness property. It is necessary to investigate the dynamic model between impedance estimation and human intention in consideration of variable stiffness. In this paper, a six-axis force/torque sensor is used to estimate the muscular efforts that the subject contributes to the end-effector, as shown in Fig. 1(b) and (c) and to predict the operator's motion in advance.

Consider an example of mechanical impedance for human limbs with an additional unknown force function $\varsigma(x, u)$ as defined in [12], i.e.,

$$f = m\ddot{x} + b\dot{x} + kx + \varsigma(x, u) \tag{3}$$

where f is the applied force, x is the steady-state displacement, m is the mass parameter, b is the damper coefficient, k is the spring stiffness, and u is internal states or inputs, however unknown. We assume that exact values of f and the position x are measurable, and the corresponding derivatives of these variables can be obtained, and the stiffness-regulating input u is bounded with its first derivative $\dot{u}$. Then, assume that the ratio between the stiffness regulation rate of change and the velocity of the trajectory measurement is bounded, for instance, for any time t during the execution of the observer, the following inequality holds $|\dot{u}(t)| < u|\dot{x}(t)|, \forall t$. Let $\frac{\partial\varsigma(x,u)}{\partial x} = \xi(x, u)$ denote the stiffness to be measured. Also, let $\hat{\xi}(t)$ denote its estimation at time t, and $\tilde{\xi} = \xi(x, u) - \hat{\xi}$ be the estimation error. Differentiating (3) once with respect to time yields

$$\dot{f} = m\dddot{x} + b\ddot{x} + k\dot{x} + \xi\dot{x} + \varsigma_u\dot{u} \tag{4}$$

where $\varsigma_u = \frac{\partial\varsigma(x,u)}{\partial u}$. Using the current estimation of stiffness and the assumptions stated above, the best possible prediction for $\dot{f}$ can be

written (in the absence of information on $\varsigma(x,u)$ and u) as $\dot{\hat{f}} = m\dddot{x} + b\ddot{x} + k\dot{x} + \dot{\hat{\xi}}\dot{x}$. The update law can be chosen as

$$\dot{\hat{\xi}} = \alpha \dot{\hat{f}} \mathrm{sgn}(\dot{x}) \tag{5}$$

with $\alpha > 0$ and $\mathrm{sgn}(\bullet) = \frac{\bullet}{\|\bullet\|}$, if $\| \bullet \| \neq 0$; else, $\mathrm{sgn}(\bullet) = 0$. It is proven that $\hat{\xi}$ can be made to converge to the true stiffness value ξ within a uniformly ultimately bounded error [13].

The traditional mass-damper-spring model used to mimic human limb dynamics [12] can be presented as $M_e(\ddot{X}_m - \ddot{X}_e) + B_e(\dot{X}_m - \dot{X}_e) + K(X_m - X_e) + \Xi = F_m$, where M_e, B_e, and K are diagonal matrices and denote the human limb mass, damper, and stiffness matrix, respectively, X_e represents the human–environment interaction location; F_m is the measured contact force, X_m is the measurement of Cartesian space coordinate of the dual-arm exoskeleton, and Ξ denotes the variable stiffness force, i.e., $\Xi = \Delta K(X_m - X_e)$ with the stiffness variation diagonal matrix ΔK, $\Xi = [\xi_1, \xi_2, \ldots, \xi_n]^T$. It is easy to calculate ΔK by using $\Delta K_i = \xi_i/(X_{mi} - X_{ei})$ if ξ_i can be obtained. In this paper, we consider the human limb stiffness as the summation of the fixed term K and the variable term Ξ. From [11] and [7], the human limb model is mainly related with the damper and spring components, and it can be simplified as

$$B_e(\dot{X}_m - \dot{X}_e) + K(X_m - X_e) + \Xi = F_m \tag{6}$$

where B_e and K are unknown impedance parameters. From (6), it is difficult to calculate X_e due to unknown B_e and K, even if F_m can be measured by a force sensor. Therefore, we need to estimate B_e and K so we can achieve the reference position X_e for the robotic exoskeleton in the task space.

Define $K_e = K + \Delta K$ and the given desired interaction force F_d, which is considered as the desired human intention. From (6) and the analytic solution of a linear first-order differential equation in [21], we can obtain $X_m = e^{-s_1 t}(C_1 + C_2 \int_0^t s_2 e^{\int_0^t s_1 dv} dt) + X_e + K_e^{-1} F_m$, where C_1 and C_2 are constants, $s_1 = \int_0^t K_e/B_e dt$ and $s_2 = B_e^{-1} F_m$ are variables. We can see that as $t \to \infty$, the position X_m tracks accurately the reference position trajectory

$$X_r = X_e + (K + \Delta K)^{-1} F_d. \tag{7}$$

If the stiffness parameters of the environment K_e and X_e are accurately known, we can synthesize the reference trajectory X_r to exert the desired contact force F_d on the environment. It should be noted that the reference trajectory X_r is generated by the human intention F_d and the human limb movement $K_e^{-1} F_d$ penetrating into the environment, which is precisely the human limb penetration needed to produce the desired human intention F_d.

However, the values of X_e, K_e, ΔK_e, and B_e are usually unknown. Let us consider using their estimations as replacement of their real values. Let $\hat{X}_e$, $\hat{K}_e$, and $\hat{B}_e$ denote the estimations of X_e, K_e, and B_e, respectively. Then, we will have the estimated reference trajectory as

$$X_r = \hat{X}_e + \hat{K}_e^{-1} F_d \tag{8}$$

where $\hat{X}_e$ and $\hat{K}_e$ are adaptively computed estimates of X_e and K_e, respectively. The measured force F_m from (6) can be written as

$$F_m = K_e X_m + B_e \dot{X}_m - F_0 \tag{9}$$

where $F_0 = K_e X_e + B_e \dot{X}_e - \Xi$, and B_e and K_e are the desired values. Considering the estimations of K_e and B_e, we have

$$\hat{F}_m = \hat{K}_e X_m + \hat{B}_e \dot{X}_m - \hat{F}_0 \tag{10}$$

where $\hat{F}_0 = \hat{K}_e \hat{X}_e + \hat{B}_e \dot{\hat{X}}_e - \hat{\Xi}$, and $\hat{X}_e$ can be viewed as a prediction of $\hat{F}_m$. Based on the current estimates of $\hat{K}_e$ and $\hat{X}_e$, from (9) and (10), we can obtain

$$\tilde{F}_m = \tilde{K}_e X_m + \tilde{B}_e \dot{X}_m - \tilde{F}_0 \tag{11}$$

where $\tilde{K}_e = \hat{K}_e - K_e$, $\tilde{B}_e = \hat{B}_e - B_e$, $\tilde{F}_m = \hat{F}_m - F_m$, and $\tilde{F}_0 = \hat{F}_0 - F_0$ are estimation errors.

Theorem 3.1: Considering the human limb dynamic model (6), we propose the following adaptation law as

$$\dot{\hat{B}}_{ei} = -\gamma_{Bi}\dot{\chi}_i \left(\hat{F}_{mi} - F_{mi}\right) \tag{12}$$

$$\dot{\hat{K}}_{ei} = -\gamma_{Ki}\chi_i \left(\hat{F}_{mi} - F_{mi}\right) \tag{13}$$

$$\dot{\hat{X}}_{ri} = \left(\hat{K}_{ei} + \hat{B}_{ei}\right)^{-1} \left(\hat{F}_{mi} - F_{mi}\right) \times \left[\gamma_{ei} + \left(\gamma_{Ki} X_{mi} + \gamma_{Bi}\dot{X}_{mi}\right)\hat{X}_{ri}\right] \tag{14}$$

$$\dot{\hat{\Xi}}_i = \alpha_i \dot{\hat{F}}_{mi} \mathrm{sgn}\left(\dot{X}_{mi} - \dot{\hat{X}}_{ei}\right) \tag{15}$$

where α_i, γ_{Bi}, and γ_{Ki} are properly selected by the designer, and the corresponding motion generation can be calculated as

$$X_{ri} = \hat{X}_{ri} + F_{di}/\hat{K}_{ei} \tag{16}$$

$$\hat{K}_{ei}(t) = \hat{K}_{ei}(0) - \gamma_{Ki}\int_0^t X_{mi}\left(\hat{F}_{mi} - F_{mi}\right) d\tau \tag{17}$$

$$\hat{B}_{ei}(t) = \hat{B}_{ei}(0) - \gamma_{Bi}\int_0^t \dot{X}_{mi}\left(\hat{F}_{mi} - F_{mi}\right) d\tau \tag{18}$$

$$\hat{F}_{mi} = \hat{K}_{ei}\left(X_{mi} - \hat{X}_{ei}\right) + \hat{B}_{ei}\left(\dot{X}_{mi} - \dot{\hat{X}}_{ei}\right) + \Xi_i \tag{19}$$

and the estimated motion intention is $\hat{X}_{ri}(t) = \hat{X}_{ri}(0) + \int_0^t (\hat{K}_{ei} + \hat{B}_{ei})^{-1}(\hat{F}_{mi} - F_{mi})(\gamma_{ei} + (\gamma_{Ki}X_{mi} + \gamma_{Bi}\dot{X}_{mi})\hat{X}_{ri})d\tau$.

Proof: See the appendix. ■

IV. Dynamics of the Dual-Arm Exoskeleton Robot

The complete dual-arm exoskeleton dynamics including the human and robot can be described in the joint space as

$$H(q)\ddot{q} + C(q,\dot{q})\dot{q} + M_g(q) + \tau_d = \tau + J_R^T \lambda \tag{20}$$

where $H(q) = \mathrm{diag}[M_A(q_A), M_B(q_B)] \in \mathbb{R}^{n\times n}$ is the block diagonal of combined inertia matrices with the subscripts A and B presenting the human arm and the exoskeleton manipulator I, and the human arm and exoskeleton manipulator II, respectively. Subsequently, we keep such notions: $C(q,\dot{q})q = \mathrm{diag}[C_A^T(q_A,\dot{q}_A)\dot{q}_A, C_B^T(q_B,\dot{q}_B)\dot{q}_B]^T \in \mathbb{R}^n$ is the combined torques of Coriolis and centrifugal forces; $M_g(q) = \mathrm{diag}[G_A^T(q_A), G_B^T(q_B)] \in \mathbb{R}^{n\times n}$ is the gravitational matrix contributed by both the human operator and exoskeleton robot; $\tau = [\tau_A^T, \tau_B^T]^T \in \mathbb{R}^n$ is the joint torque vector of dual arms; $\tau_d \in \mathbb{R}^n$ is the unknown mechanical disturbance. The robot's end-effector in the relative motion can be viewed as restricting only the dynamics on an equivalent constraint manifold Ω_h defined by [22] $\Omega_h = \{(q,\dot{q}) | h(q) = 0 \in \mathbb{R}^l, J_R(q)\dot{q} = 0\}$. The constraint force can be measured by a force sensor on the end-effector and can be converted into joint space as $f = J_R^T(q)\lambda \in \mathbb{R}^n$ where $J_R(q) = \frac{\partial h}{\partial q} \in \mathbb{R}^{l\times n}$ with $l = 6$, where $\lambda \in \mathbb{R}^l$ is a generalized Lagrangian multiplier.

Inspired by the implicit function theorem in [10], there exists a proper partition of q, i.e., $q = [{q_1}^T, {q_2}^T]^T$ for $q_1 \in \mathbb{R}^{n-l}$, and $q_2 \in \mathbb{R}^l$, such that $h(q) = 0$ can be rewritten as $q_2 = \Omega(q_1)$ with a nonlinear mapping function Ω. Considering the partition $\dot{X}_{co} = J_R(q)\dot{q}$, we can derive $\dot{X}_{co} = [\dot{X}_1^T, \dot{X}_2^T]^T$ and $J_R(q) = \mathrm{diag}[J_1(q), J_2(q)]$, $\dot{X}_1 = J_1\dot{q}_1$, $\dot{X}_2 = J_2\dot{q}_2$. One can obtain that the

terms $\partial\Omega/\partial q_1$ and $\partial^2\Omega/\partial(q_1)^2$ are bounded. Moreover, we have the following relationship for the independent coordinates $q_1, \dot{q}_1$ as $q = [(q_1)^T, \Omega(q_1)^T]^T$, $\dot{q} = [I_{n-l}, \frac{\partial\Omega(q_1)}{\partial q_1}]^T \dot{q}_1 = A(q_1)\dot{q}_1$. Differentiating the constraint $h(q) = 0$ with regard to time t, we have $J_R(q)A(q_1)\dot{q}_1 = 0$. Noting that $\dot{q}_1$ is an independent coordinate, we have $J_R(q)A(q_1) = 0$ and $A^T(q_1)J_R^T(q) = 0$. Due to the velocity transformation, the derivatives of $\dot{q}$ should satisfy $\ddot{q} = A(q_1)\ddot{q}_1 + \dot{A}(q_1)\dot{q}_1$.

To simplify the notations, we will omit variables in function vectors or matrices in the rest of this paper. For example, without causing ambiguity, we will use H, C, M_g, h, and A to denote $H(q)$, $C(q,\dot{q})$, $M_g(q)$, $h(q)$, and $A(q_1)$, respectively. Then, we can have

$$HA\ddot{q}_1 + (CA + H\dot{A})\dot{q}_1 + M_g + \tau_d = \tau + J_R^T\lambda \tag{21}$$

Multiplying A^T by both sides of (21), we can obtain

$$\mathcal{H}\ddot{q}_1 + \mathcal{C}\dot{q}_1 + \mathcal{G} + \mathcal{T}_d = \mathcal{T} \tag{22}$$

with $\dot{X}_1 = J_1\dot{q}_1$, where $\mathcal{H} = A^T HA \in \mathbb{R}^{(n-l)\times(n-l)}$, $\mathcal{C} = A^T(CA + H\dot{A}) \in \mathbb{R}^{(n-l)\times(n-l)}$, $\mathcal{G} = A^T M_g \in \mathbb{R}^{n-l}$, $\mathcal{T}_d = A^T\tau_d \in \mathbb{R}^{n-l}$, and $\mathcal{T} = A^T\tau \in \mathbb{R}^{n-l}$.

Property 4.1: [10] The $\mathcal{H}$ and its inverse $\mathcal{H}^{-1}$ are positive and symmetric definite matrices, and the $\dot{\mathcal{H}} - 2\mathcal{C}$ is a skew-symmetric matrix.

V. Control Design

Defining error variables $e_1 = X_1 - X_{1d}$, and $e_2 = \dot{q}_1 - \vartheta_1$, with a virtual input can be designed as

$$\vartheta_1 = J_1^+(q)\left[-\cos^2\left(\frac{\pi e_1^T e_1}{2\varepsilon^2}\right)K_1 e_1 + \dot{X}_{1d}\right] \tag{23}$$

where ε denotes a designed small positive constant.

The human joints have physical limits, and to avoid possible danger to the human during the motion, the constraint of tension should be considered in the control design. Therefore, errors e_1 and e_2 are required to remain in their respective constraint set $\Omega_1 = \{\|e_1\| < \varepsilon\}$ and $\Omega_2 = \{\|e_2\| < \varrho\}$. It should be noted that due to the nonsingularity assumption, the pseudoinverse J_1^+ exists, and $J_1 J_1^+ = I$. In order to assure the constraints for e_1, and the corresponding X_1, where $\dot{X}_1 = J_1\dot{q}_1$, we need to guarantee that e_1 and e_2 do not transgress the constrained region.

Consider the following desired control law

$$\mathcal{T}^* = \mathcal{T}_a^* + \mathcal{T}_b^* \tag{24}$$

$$\mathcal{T}_a^* = -\cos^2\left(\frac{\pi e_2^T\mathcal{H}e_2}{2\varrho^2}\right)\left(\frac{J_1^T e_1}{\cos^2\left(\frac{\pi e_1^T e_1}{2\varepsilon^2}\right)} + K_2 e_2\right) \tag{25}$$

$$\mathcal{T}_b^* = \mathcal{H}\dot{\vartheta}_1 + \mathcal{C}\vartheta_1 + \mathcal{G} + \mathcal{T}_d \tag{26}$$

where ϱ denotes the constraint on e_2 and can be designed as a small positive constant, K_2 is a positive-definite constant matrix to be designed. $\mathcal{T}_a^*$ and $\mathcal{T}_b^*$ can be respectively interpreted as a control input for constraints and a control input that deals with the dynamics of the robot. Since $\mathcal{H}$, $\mathcal{C}$, $\mathcal{G}$, and $\mathcal{T}_d$ cannot be obtained beforehand, the designed control law (24) cannot be implemented, therefore, we have the following property.

Property 5.1: Define $\Psi = \mathcal{H}\dot{\vartheta}_1 + \mathcal{C}\vartheta_1 + \mathcal{G} + \mathcal{T}_d$, and there exist some unknown finite nonnegative constants $c_i \geq 0 (i = 1, 2, 3, 4)$ such that $\forall q \in R^n$, $\forall \dot{q} \in R^n$, $\|\mathcal{H}\dot{\vartheta}_1\| \leq c_1\|\dot{\vartheta}_1\|$, $\|\mathcal{C}\vartheta_1\| \leq c_2\|\dot{q}\|\|\vartheta_1\|$, $\|\mathcal{G}\| \leq c_3$ and $\|\mathcal{T}_d\| \leq c_4$.

Define $\beta_1 = \cos^2(\frac{\pi\lambda_{\max}e_2^T e_2}{2\varrho^2})$, $\beta_2 = \cos^2(\frac{\pi\lambda_{\min}e_2^T e_2}{2\varrho^2})$.

Definition 5.1: Consider a time-varying positive function $\delta(t)$ that converges to zero as $t \to \infty$ and satisfies $\lim_{t\to\infty}\int_0^t \delta(s)ds = b < \infty$, with finite constant b. For example, $\delta(t) = 1/(1+t)^2$.

Consider the adaptive robust approach

$$\mathcal{T} = \mathcal{T}_a + \mathcal{T}_b \tag{27}$$

$$\mathcal{T}_a = -\frac{\beta_1 J_1^T e_1}{\cos^2\left(\frac{\pi e_1^T e_1}{2\varepsilon^2}\right)} - \beta_2 K_2 e_2 \tag{28}$$

$$\mathcal{T}_b = -\frac{\beta_2}{\beta_1}\sum_{i=1}^{4}\frac{|\hat{c}_i|\Phi_i^2 e_2}{\Phi_i\|e_2\| + \beta_1\omega_i} \tag{29}$$

where K_2 is a positive-definite constant matrix; $\hat{c}_i$ is the estimation of c_i; ω_i satisfies Definition 5.1, and $\lim_{t\to\infty}\int_0^t \omega_i(s)ds = b_{1i} < \infty$ with positive constants $b_{1i} (i = 1, 2, 3, 4)$; $\Phi = [\|\dot{\vartheta}_1\|, \|\dot{q}\|\|\vartheta_1\|, 1, 1]^T \in \mathbb{R}^6$. Similar to model-based controller (24), $\mathcal{T}_a$ and $\mathcal{T}_b$ are control inputs for constraints and the uncertain dynamics of the robot, respectively.

The corresponding adaptive updating law is $\dot{\hat{c}}_i = -\Gamma_i(\sigma_i\hat{c}_i - \frac{\Phi_i^2\|e_2\|^2}{\beta_1(\Phi_i\|e_2\| + \beta_1\omega_i)})$, where Γ_i is a positive constant to be designed; σ_i satisfies Definition 5.1, and $\lim_{t\to\infty}\int_0^t \sigma_i(s)ds = b_{2i} < \infty$ with positive constants b_{2i}. The stability of the proposed controller (27) with the adaptive law is analyzed in the appendix.

The designed controller (27) only contains motion control law. For force control, we need to design the force controller. Considering (21), let us derive the force λ as

$$\lambda = Z[(CA + H\dot{A})\dot{q}_1 + M_g + \tau_d - \tau] \tag{30}$$

where $Z = (J_R H^{-1} J_R^T)^{-1} J_R H^{-1}$. Consider the overall control input $\tau = \tau_m + J_R^T\tau_f$ with the motion control τ_m satisfying $\tau_m = A^{+T}\mathcal{T}$ (A^+ is the left inverse of A^T, which can be calculated by $A^+ = A(A^T A)^{-1}$) and the force control τ_f, one can obtain

$$\lambda = Z[(CA + H\dot{A})\dot{q}_1 + M_g + \tau_d + \tau_h - \tau_m] - \tau_f \tag{31}$$

The force control law is designed as

$$\tau_f = \lambda_d - K_f e_\lambda \tag{32}$$

where K_f is a designed parameter, $e_\lambda = \lambda - \lambda_d$. Substituting (32) into (31), we have

$$(K_f + I)e_\lambda = Z[(CA + H\dot{A})\dot{q}_1 + M_g + \tau_d - \tau_m] \tag{33}$$

Theorem 5.1: Consider the dynamics of dual-arm exoskeleton (22), the adaptive controller (27) and the update law $\dot{\hat{c}}_i$. If the initial errors satisfy $\|e_1(0)\| < \varepsilon$ and $\|e_2(0)\| < \varrho$, then the following conclusions can be made.

1) All the closed-loop signals are bounded.
2) $\forall t > 0$, the constraints $\|e_1(t)\| < \varepsilon$ and $\|e_2(t)\| < \varrho$ hold, where ε and ϱ are two small positive constants to be designed.
3) The position $X_1(t)$ of the end-effector satisfies $\underline{X}_1(t) < X_1(t) < \overline{X}_1(t)$ with the upper and lower limits $\overline{X}_1(t) = -\varepsilon + X_{1d}(t)$ and $\underline{X}_1(t) = \varepsilon + X_{1d}(t)$, respectively, $\forall t > 0$, which makes the constraints nonviolated.
4) The tracking errors $e_1(t)$ and $e_2(t)$ and $e_\lambda(t)$ converge to the origin, i.e., $X(t) \to X_{1d}(t)$, $\dot{q}_1(t) \to \vartheta$.
5) The force tracking error e_λ is bounded as $t \to \infty$.

Proof: See the appendix. ■

VI. Experiments

The developed dual-arm exoskeleton robot consists of two 5-DOF exoskeleton platforms shown in Fig. 1(b). There are five revolute

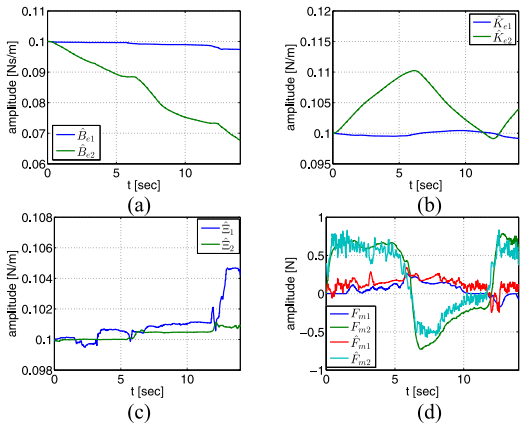

Fig. 2. Experimental results of subject 1. (a) Adaptive update of damping parameter $\hat{B}_e$. (b) Adaptive update of stiffness parameter $\hat{K}_e$. (c) Update of variable stiffness $\hat{\Xi}$. (d) Interaction force and their estimation in the task operation.

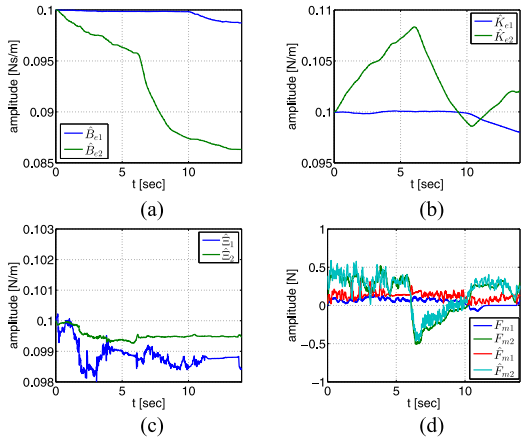

Fig. 3. Experimental results of subject 3. (a) Adaptive update of damping parameter $\hat{B}_e$. (b) Adaptive update of stiffness parameter $\hat{K}_e$. (c) The update of variable stiffness $\hat{\Xi}$. (d) The interaction force and their estimation in the task operation.

joints in the developed exoskeleton. Motors 1–5 are used for shoulder abduction–adduction, shoulder flexion–extension, elbow flexion–extension, forearm pronation–supination and wrist radial–ulnar deviation, respectively. By using (12) and (13), we can estimate the human intention X_r in (16). Therefore, a force sensor needs to be used to measure the interactive force between human and the dual-arm exoskeleton robot, as shown in Fig. 1(c), which is mounted on the end-effector of the right arm.

A drawing task is considered in the experiment as shown in Fig. 1(b). The left arm moves according to the predetermined trajectory on the circular object held by the end-effector of the right arm. Five joints/DOFs are involved in the experiment, i.e., three joints/DOFs of the left arm to perform drawing task, and two joints/DOFs of the right arm to maintain the circular object. The left arm maintains the contact during the drawing. During execution of the task, the desired relative trajectories are designed to keep the end-effector of the left arm perpendicular to the surface of the circular object, which is held by the end-effector of the right arm. A constant force is exerted in vertical direction on the circular object. We first predefine a time-varying target trajectory and second employ the designed human intention estimation method to recognize the human's real intention and then drive the dual-arm exoskeleton robot to follow the recognized human intention by the developed adaptive control strategy. Specifically, the shoulder joint of the exoskeleton robot's left arm is constrained between two predefined target positions, whereas the elbow joint of the exoskeleton robot's left arm is expected to be constrained between another two predefined target positions. The same experiment was repeatedly performed five times with five different subjects whose information are Subject 1 (male; age: 24; height: 165 cm; weight: 59 kg), Subject 2 (male; age: 25; height: 181 cm; weight: 65 kg), Subject 3 (male; age: 24; height: 172 cm; weight: 72 kg), Subject 4 (female; age: 23; height: 160 cm; weight: 45 kg), and Subject 5 (female; age: 28; height: 158 cm; weight: 51 kg). Due to the similarity of the experimental results and page limits, we only present the results of Subjects 1, 3, and 5.

The results of the three subjects are shown in Figs. 2–9. First, Subject 1's experimental results are shown in Figs. 2 and 5. The estimations of the human arm, i.e., B_e, K_e, and Ξ, are updated in Figs. 2(a)–(c). The interaction force and its estimation are shown in Fig. 2(d). The estimated human intention trajectories for the end-effector are shown in Fig. 5. The figure illustrates that the end-effector tracks the de-

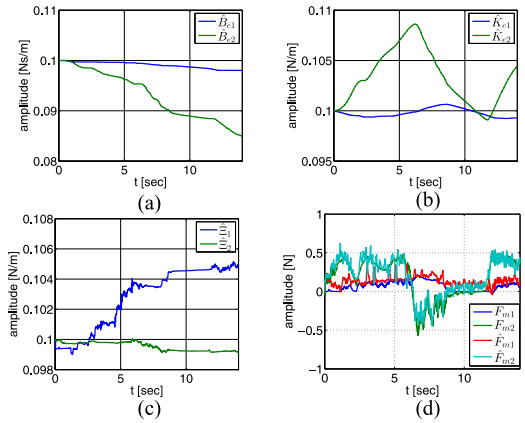

Fig. 4. Experimental results of subject 5. (a) Adaptive update of damping parameter $\hat{B}_e$. (b) Adaptive update of stiffness parameter $\hat{K}_e$. (c) Update of variable stiffness $\hat{\Xi}$. (d) Interaction force and their estimation in the task operation.

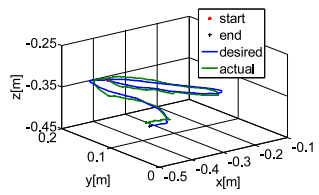

Fig. 5. Relative trajectories of the end-effector for Subject 1.

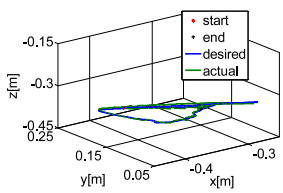

Fig. 6. Relative trajectories of the end-effector for Subject 3.

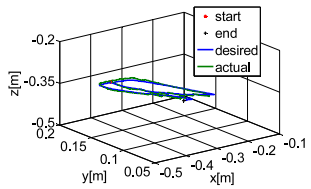

Fig. 7. Relative trajectories of the end-effector for Subject 5.

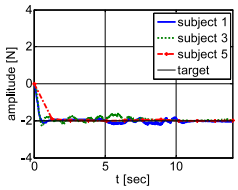

Fig. 8. External force exerted on the circular object holding by arm II's end-effector.

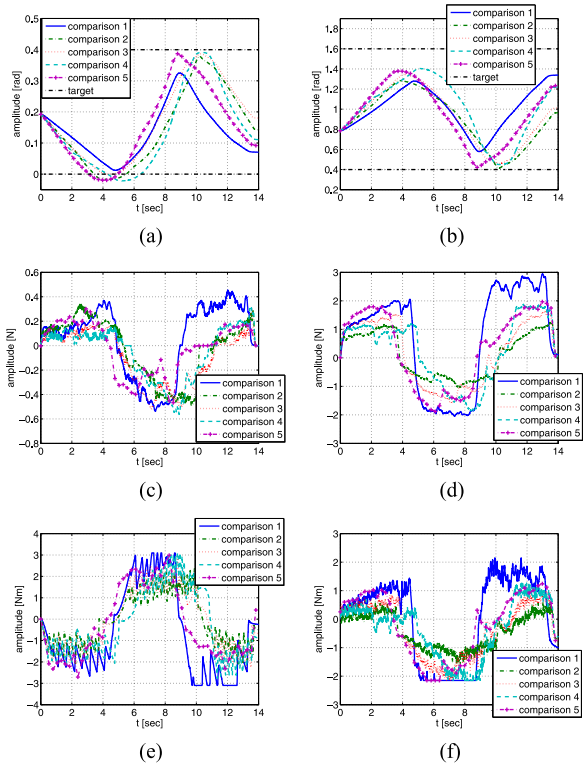

Fig. 9. Comparative experimental results of Subjects 1–5. (a) Trajectories of the exoskeleton shoulder joint. (b) Trajectories of the exoskeleton elbow joint. (c) Interaction force $F_{m\,1}$. (d) Interaction force $F_{m\,2}$. (e) Input torque of the exoskeleton shoulder joints. (f) Input torque of the exoskeleton elbow joints.

sired trajectory with sufficiently small tracking errors. It is obvious that the tracking errors are smaller as time evolves. From these figures, the desired performance is obtained by using the proposed control scheme, even if little dynamics knowledge of the exoskeleton and the external disturbances in the environment is available. Moreover, in order to make an evaluation of the coincidence between the interaction force and its estimation (10), a metric is employed: $D = \frac{1}{N}\sum_{i=1}^{N}\sqrt{(F_{m\,1}(i)-\hat{F}_{m\,1}(i))^2+(F_{m\,2}(i)-\hat{F}_{m\,2}(i))^2}$, where N is the sampling data number in experiments, and i denotes the ith sampling point. The definition of the metric is able to quantitatively describe

TABLE I
METRIC VALUES BETWEEN THE INTERACTION FORCES AND ESTIMATIONS

Subject no.	1	3	5
Metric value	0.1738	0.1079	0.1146

TABLE II
PERFORMANCE INDICES

Joints	Controllers	$L_2(e)$	e_F	$L_2(U)$	U_m
Shoulder joint	Proposed	0.0219	0.0243	1.3096	1.7309
	Conventional	0.0849	0.0820	5.1992	3.1000
Elbow joint	Proposed	0.0230	0.0119	0.6496	1.4991
	Conventional	0.1635	0.0289	3.6840	2.1500

the estimation errors of the human subjects' motion intention, so the metric values are used to evaluate the performance of the experiments.

Figs. 3 and 4 and Figs. 6 and 7 show the results of Subjects 3 and 5, respectively. From these figures, we observe that the dual-arm exoskeleton is able to recognize the human intention by the proposed human intention estimation method and also can track the desired human intention trajectory effectively by the proposed adaptive control strategy. The external force exerted on the circular object held by arm II's end-effector is shown in Fig. 8. We can observe that the actual external force λ tracks the target force λ_d with small tracking error as shown in Fig. 8 for all the five subjects and the trajectory of λ shows the tendency of converging to the target force λ_d. The metric values of Subjects 1, 3, and 5 are shown in Table 1.

We also perform a comparison experiment using the conventional impedance control method. In the comparative experiment, we choose the impedance parameters as $M_d = \mathrm{diag}[0.0, 0.0]$, $B_d = \mathrm{diag}[7.0, 6.0]$, and $K_d = \mathrm{diag}[0.1, 0.1]$. The controller parameters are chosen as $K_1 = \mathrm{diag}[27.45, 25.8]$, $K_2 = \mathrm{diag}[8.01, 6.4]$, $\varepsilon = 0.03$, $\varrho = 2$, $\lambda_{\max} = 3.5336$, $\lambda_{\min} = 0.08$, and $\omega_j = 5/(t+1)^2$. The force controller parameter in (32) is chosen as $K_f = 5$. The target external force is $\lambda_d = -2.0N$. We choose $\hat{c}_i = 0 (i = 1, 2, 3, 4)$ as the initial values of adaptive laws. Parameters in adaptive laws are set to $\Gamma_i = 0.15$ and $\sigma_i = 2/(t+1)^2$. The interaction force is measured by a force sensor mounted on the end-effector of the right arm. The design parameters with regard to the human arm model are chosen as $\gamma_{K\,i} = 0.1$, $\gamma_{B\,i} = 0.1$, and $\gamma_{e\,i} = 0.01$. Moreover, our controller is designed at the torque level. Since the motor current is proportional to the motor torque and the current values from the motor drivers can be measured, we therefore use the input currents as control signals to track the desired currents, which are obtained by transferring the desired torques into the desired currents. This explains how the control law is designed at the torque level and why the results in the figures use currents as input signals.

The results of comparative experiments among all five subjects using the traditional impedance control method presented in [7] are shown in Fig. 9. The five lines in every figure denote the experiment result of each subject. The estimated human intention for exoskeleton shoulder and elbow joints are presented in Fig. 9(a) and (b). Fig. 9(c) and (d) shows the measured interaction force in the experiment process. The input torque for the two joints are shown in Fig. 9(e) and (f). From Figs. 2–4 and 9(c) and (d), we observe that when using our human intention identification scheme, the interactive force between the exoskeleton robot arm and its human partner is smaller. In the comparative experiment, we used the same impedance parameters for all the five subjects.

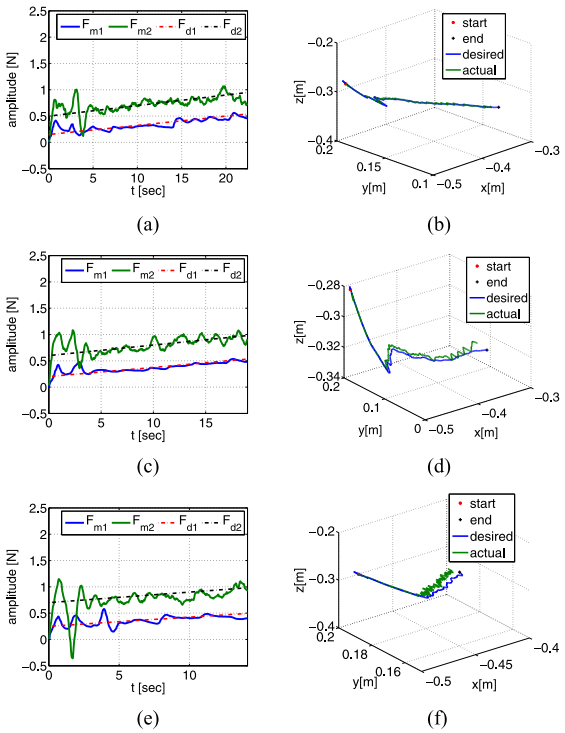

Fig. 10. Experimental results of subject 1, 3, and 5. (a) Interaction force of subject 1. (b) Relative trajectories of the end-effector of subject 1. (c) Interaction force of subject 3. (d) Relative trajectories of the end-effector of subject 3. (e) Interaction force of subject 5. (f) Relative trajectories of the end-effector of subject 5.

Moreover, we have compared the intersubject experimental results in Figs. 2–4. From these figures, we see that the estimated human arm parameters B_e, K_e, and Ξ are considerably different. It is understandable because different human subjects should have different arm parameters. Though the human arm parameters cannot be identified exactly, we can approximate the human arm parameters using our method proposed in Section III. The damping parameter $\hat{B}_e$ and the stiffness parameter $\hat{K}_e$ are calculated by the adaptation law (12) and (13), respectively. Then, the parameters can be approximated by (17) and (18). The proposed adaptation laws show that the estimated impedance parameters are able to make $\hat{F}_m \to F_m$ and $F_m \to F_d$, which is proved in the appendix. This demonstrates that the parameters can be used to obtain human intention. The experimental results verify that the developed method is able to estimate the desired human intention F_d while the motion tracking errors are convergent in the meantime.

The following performance indices are used to measure the quality of the proposed control method. The statistics are presented in Table 2.

1) The scalar-valued norm $L_2[e] = \sqrt{(\frac{1}{T_f})\int_0^{T_f} |e|^2 dt}$ is used as an objective numerical measure of the average tracking performance for the entire error $e(t)$, where T_f is the total running time.
2) The maximal absolute value of the tracking error $e_F = \max_{T_f-2\le t\le T_f} |e(t)|$ during the last 2 s is used as an index of measure of the final tracking accuracy.
3) The average input torque $L_2[U] = \sqrt{(\frac{1}{T_f})\int_0^{T_f} |U|^2 dt}$ is used to evaluate the amount of control efforts.
4) The maximal absolute value of the control effort $U_m = \max |U(t)|$ is used as an index of measure of the transient performance.

In addition, an extra group of experiments are added and the results are shown in Fig. 10. In the experiments, the human intention F_d is set as a time-varying function. The human subjects follow the predefined trajectory drawn on the board and the interaction force would converge to F_d, which indicates that human intention is estimated, as shown in Fig. 10(a), (c), and (e). The estimated human intention trajectories for the end-effector are shown in Fig. 10(b), (d), and (f). When the desired interaction forces F_d become larger, the velocities of the manipulator would increase more rapidly, so the completion times would decrease. The desired interaction forces F_d and the completion times t_c of the subjects are as follows: Subject 1 ($F_{d1} = (0.15 + 0.02\,t)N$, $F_{d2} = (0.5 + 0.02\,t)N$, $t_c = 22.4\,s$), Subject 3 ($F_{d1} = (0.2 + 0.02\,t)N$, $F_{d2} = (0.6 + 0.02t)N$, $t_c = 19.2\,s$), and Subject 5 ($F_{d1} = (0.25 + 0.02\,t)N$, $F_{d2} = (0.7 + 0.02t)N$, $t_c = 14.1\,s$).

VII. Conclusion

This paper developed a BLF-based adaptive impedance control for dual-arm exoskeleton with unknown intention of the human operator, unknown robot dynamics, and physical limits. The motion intention of the human operator is considered as the desired trajectory, and impedance parameter online approximation is employed to deal with the nonlinear and variable stiffness property of the human limb model. Experiments have been conducted to demonstrate that the proposed dual-arm coordination controller is effective. In the future work, we plan to take stroke patients as participants in the experiments to test control performance of our design.

Appendix

Consider the barrier composite energy function candidate as $V = \frac{\varepsilon^2}{\pi}\tan(\frac{\pi e_1^T e_1}{2\varepsilon^2}) + \frac{\varrho^2}{\pi}\tan(\frac{\pi e_2^T \mathcal{H} e_2}{2\varrho^2}) + \frac{1}{2}\sum_{i=1}^4 \frac{1}{\Gamma_i}\tilde{c}_i^2 + \sum_{i=1}^n \frac{1}{2\gamma_{Bi}}\tilde{B}_{ei}^2 + \sum_{i=1}^n \frac{1}{2\gamma_{Ki}}\tilde{K}_{ei}^2 + \sum_{i=1}^n \frac{1}{2\gamma_{ei}}\tilde{F}_{0i}^2$, where $\tilde{c}_i = \hat{c}_i - c_i$. Considering the derivative of V, using Property 4.1 and (12) and (13), and by defining $\dot{\tilde{F}}_{0i} = \gamma_{ei}(\hat{F}_{mi} - F_{mi})$, we have $\dot{V} \le -e_1^T K_1 e_1 + \frac{e_1^T J_1 e_2}{\cos^2(\frac{\pi e_1^T e_1}{2\varepsilon^2})} - \frac{e_2^T}{\cos^2(\frac{\pi e_2^T \mathcal{H} e_2}{2\varrho^2})}(\mathcal{C}\vartheta_1 + \mathcal{G} + \mathcal{T}_d + \mathcal{H}\dot{\vartheta}_1) + \frac{e_2^T \mathcal{T}}{\cos^2(\frac{\pi e_2^T \mathcal{H} e_2}{2\varrho^2})} + \sum_{i=1}^4 \frac{1}{\Gamma_i}\tilde{c}_i\dot{\tilde{c}}_i$. Since $0 \le \cos^2(\frac{\pi \lambda_{\max} e_2^T e_2}{2\varrho^2}) \le \cos^2(\frac{\pi e_2^T \mathcal{H} e_2}{2\varrho^2}) \le \cos^2(\frac{\pi \lambda_{\min} e_2^T e_2}{2\varrho^2}) \le 1$, integrating (27) into $\dot{V}$, considering Property 5.1, and using the fact of $-\beta_2/\cos^2(\frac{\pi e_2^T \mathcal{H} e_2}{2\varrho^2}) \le -1$, we can rewrite $\dot{V}$ as $\dot{V} \le -e_1^T(K_1 - \alpha/(2\cos^2(\frac{\pi e_1^T e_1}{2\varepsilon^2})))e_1 - e_2^T(K_2 - \alpha/(2\cos^2(\frac{\pi e_1^T e_1}{2\varepsilon^2})))e_2 + \frac{e_2^T \mathcal{T}_b - e_2^T \Psi}{\cos^2(\frac{\pi e_2^T \mathcal{H} e_2}{2\varrho^2})}$, where $\alpha = \|J_1\|(1 - \frac{\beta_1}{\beta_2})$. Considering the following inequality, which is bounded by $\frac{e_2^T \mathcal{T}_b}{\cos^2(\frac{\pi e_2^T \mathcal{H} e_2}{2\varrho^2})} - \frac{e_2^T \Psi}{\cos^2(\frac{\pi e_2^T \mathcal{H} e_2}{2\varrho^2})} + \frac{1}{2}\sum_{i=1}^4 \Gamma_i^{-1}\tilde{c}_i\dot{\tilde{c}}_i \le \sum_{i=1}^4 c_i\omega_i - \sum_{i=1}^4 \frac{1}{2}\sigma_i\tilde{c}_i\tilde{c}_i + \sum_{i=1}^4 \frac{1}{2}\sigma_i c_i^2$, where we use the facts: $-\beta_2/\cos^2(\frac{\pi e_2^T \mathcal{H} e_2}{2\varrho^2}) \le -1$, $\frac{\beta_1 c_i \Phi_i \|e_2\|\omega_i}{\Phi_i\|e_2\| + \beta_1\omega_i} \le \beta_1 c_i\omega_i$, and $-|\hat{c}_i| \le -\hat{c}_i$ $(i = 1, \ldots, 4)$, the last inequality obtained is because $-\tilde{c}_i\hat{c}_i = -\tilde{c}_i(c_i + \tilde{c}_i) = -\tilde{c}_i\tilde{c}_i - \tilde{c}_i c_i$, and $-\tilde{c}_i c_i \le \frac{1}{2}(\tilde{c}_i\tilde{c}_i + c_i c_i)$, we have $-\tilde{c}_i\hat{c}_i \le -\frac{1}{2}\tilde{c}_i\tilde{c}_i + \frac{1}{2}c_i c_i$. Then, we can rewrite $\dot{V}$ as $\dot{V} \le -e_1^T(K_1 - \alpha/(2\cos^2(\frac{\pi e_1^T e_1}{2\varepsilon^2})))e_1 - e_2^T(K_2 - \alpha/(2\cos^2(\frac{\pi e_1^T e_1}{2\varepsilon^2})))e_2 + \sum_{i=1}^4 c_i\omega_i + \sum_{i=1}^4 \frac{1}{2}\sigma_i c_i^2 - \sum_{i=1}^4 \frac{1}{2}\sigma_i\tilde{c}_i\tilde{c}_i$. Since $\sum_{i=1}^4 c_i\omega_i \to 0$ and $\sum_{i=1}^4 \frac{1}{2}\sigma_i c_i^2 \to 0$ as $t \to \infty$ due to the definition of ω_i and σ_i, and by selecting the suitable positive-definite constant matrices K_1, K_2 satisfying $K_1 \ge \frac{\alpha}{2}I$ and $K_2 \ge \frac{\alpha}{2}I$, and positive con-

stants $\Gamma_i (i = 1, \ldots, 4)$. Thus, e_1 and e_2 converge to the origin as $t \to \infty$. Integrating both sides of the above equation gives $V(t) - V(0) \leq -\int_0^t \{e_1^T (K_1 - \alpha/(2\cos^2(\frac{\pi e_1^T e_1}{2\varepsilon^2})))e_1 + e_2^T (K_2 - \alpha/(2\cos^2(\frac{\pi e_1^T e_1}{2\varepsilon^2})))e_2 + \sum_{j=1}^4 \frac{1}{2}\sigma_j \tilde{c}_j \tilde{c}_j\} ds + \int_0^t \{\sum_{i=1}^4 c_i \omega_i + \sum_{i=1}^4 \frac{1}{2}\sigma_i c_i^2\} ds$. Since c_i is constant, $\int_0^\infty \omega_i ds = b_{1i}$ and $\int_0^\infty \sigma_i ds = b_{2i} (i = 1, \ldots, 4)$ are constants, we can rewrite it as $V(t) - V(0) < \infty$. Thus, V is bounded such that $e_1, e_2 \in L_\infty$, and $X \in L_\infty$ according to the boundedness of X_{1d}. We can conclude that J_1 and q are bounded. Since c_i is a constant, we have $\hat{c}_i$ that is also bounded.

1) Since the augmented Lyapunov function V is bounded, it is obvious that all the closed-loop signals are bounded.
2) Assume that there exists $t = T$ such that $\|e_1(t)\|$ or $\|e_2(t)\|$ grows to their respective constraint ε or ϱ, i.e., $\|e_1(T)\| = \varepsilon$ or $\|e_2(T)\| = \varrho$. The initial values $\|e_1(0)\| < \varepsilon$ and $\|e_2(0)\| < \varrho$. Then, we obtained the conclusion that V rises infinitely by substituting $e_1(T)$ or $e_2(T)$ into $\dot{V}$. However, V is bounded. According to the method of proof by contradiction, we have the constraints $\|e_1(t)\| < \varepsilon$ and $\|e_2(t)\| < \varrho$ holding for $\forall t > 0$.
3) We have $\|e_1(t)\| < \varepsilon$ from 2). From the definition of $e_1(t)$, we have $X_1(t) = e_1(t) + X_{1d}(t)$. Then, we have $-\varepsilon + X_{1d}(t) < X_1(t) < \varepsilon + X_{1d}(t)$, which indicates $\underline{X}_1(t) < X_1(t) < \overline{X}_1(t)$ where $\overline{X}_1(t) = -\varepsilon + X_{1d}(t)$ and $\underline{X}_1(t) = \varepsilon + X_{1d}(t)$.
4) According to the Definition 5.1, we have $\omega_j \to 0$ and $\sigma_j \to 0 (j = 1, \ldots, 4)$ as $t \to \infty$. We have $\dot{V} \leq 0$ as $t \to \infty$ by choosing appropriate design parameters K_1, K_2 and $\Gamma_j (j = 1, \ldots, 4)$, $X(t) \to X_{1d}(t)$ and $\dot{q}_1(t) \to \vartheta$.
5) Since $e_2 = \dot{q}_1 - \vartheta_1$ and ϑ_1 are bounded, $\dot{q}_1$ is also bounded. Then, Z, C, A, $\dot{A}$, M_g, τ_h, and τ_m in (33) are both bounded. Considering the bounded H and $\dot{q}_1$, we obtain that the right-hand side of (33) is bounded. In other words, $(K_f + I)e_\lambda$ is bounded. Then, the force error e_f is bounded.

REFERENCES

[1] M. Trlep, M. Mihelj, and M. Munih, "Skill transfer from symmetric and asymmetric bimanual training using a robotic system to single limb performance," *J. Neuroeng. Rehabil.*, vol. 9, no. 43, 2012, pp. 1–14.

[2] Z. Li, P. Tao, S. S. Ge, M. D. Adams, and W. S. Wijesoma, "Robust adaptive control of cooperating mobile manipulators with relative motion," *IEEE Trans. System, Man, Cybern., Part B*, vol. 39, no. 1, pp. 103–116, Feb. 2009.

[3] Z. Li *et al.*, "Decentralized adaptive control of cooperating mobile manipulators with disturbance observers," *IET Control Theory Appl.*, vol. 8, no. 7, pp. 515–521, May 2014.

[4] W. S. Owen, E. A. Croft, and B. Benhabib, "Acceleration and torque redistribution for a dual-manipulator system," *IEEE Trans Robot.*, vol. 21, no. 6, pp. 1226–1230, Dec. 2005.

[5] J. Lee, P. H. Chang, and R. S. Jamisola, "Relative impedance control for dual-arm robots performing asymmetric bimanual tasks," *IEEE Trans. Ind. Electron.*, vol. 61, no. 7, pp. 3786–3796, Jul. 2014.

[6] R. Riener, L. Lunenburger, S. Jezernik, M. Anderschitz, G. Colombo, and V. Dietz, "Patient-cooperative strategies for robot-aided treadmill training: First experimental results," *IEEE Trans. Neural Syst. Rehabil. Eng.*, vol. 13, no. 3, pp. 380–394, Sep. 2005.

[7] Y. Li and S. S. Ge, "Human–robot collaboration based on motion intention estimation," *IEEE/ASME Trans. Mechatronics*, vol. 19, no. 3, pp. 1007–1014, Jun. 2014.

[8] K. P. Tee, S. S. Ge, E. H. Tay, "Barrier Lyapunov functions for the control of output-constrained nonlinear systems," *Automatica*, vol. 45, no. 4, pp. 918–927, Apr. 2009.

[9] K. P. Tee, B. Ren, and S. S. Ge, "Control of nonlinear systems with time-varying output constraints," *Automatica*, vol. 47, no. 11, pp. 2511–2516, Nov. 2011.

[10] Z. Li and S. S. Ge, *Fundamentals in Modeling and Control of Mobile Manipulators*, Boca Raton, FL, USA: CRC Press, May 2013.

[11] D. Erickson, M. Weber, I. Sharf, "Contact stiffness and damping estimation for robotic systems," *Int. J. Robot. Res.*, vol. 22, no. 1, 2003, pp. 41–57.

[12] M. Rahman, R. Ikeura, and K. Mizutani, "Investigation of the impedance characteristic of human arm for development of robots to cooperate with humans," *JSME Int. J. Ser. C*, vol. 45, no. 2, pp. 510–518, 2002.

[13] G. Grioli and A. Bicchi, "A non-invasive, real-time method for measuring variable stiffness," in *Proc. Robot. Sci. Syst.*, Zaragoza, Spain, 2010, pp. 89–96.

[14] F. Flacco, A. De Luca, I. Sardellitti, N. G Tsagarakis, "On-line estimation of variable stiffness in flexible robot joints," *Int. J. Robot. Res.*, vol. 31, no. 13, 1556–1577, Nov. 2012.

[15] T. Menard, G. Grioli, A. Bicchi, "A real time robust observer for an agonist-antagonist variable stiffness actuator," in *Proc. Int. Conf. Robot. Autom.*, 2013, pp. 3988–3993.

[16] G. Grioli, A. Bicchi, "A real-time parametric stiffness observer for VSA devices," in *Proc. Int. Conf. Robot. Autom.*, 2011, pp. 5535–5540.

[17] M. W. Spong, and M. Vidyasagar, *Robot Dynamics and Control*, New York, NY, USA: Wiley, 1989.

[18] V. Duchaine and C. Gosselin, "General model of human–robot cooperation using a novel velocity based variable impedance control," in *Proc. 2nd Joint EuroHaptics Conf. Symp. Haptic Interfaces Virtual Environ. Teleoperator Syst.*, pp. 446–451, 2007.

[19] K. Wakita, J. Huang, P. Di, K. Sekiyama, and T. Fukuda, "Human-walking-intention-based motion control of an omnidirectional-type cane robot," *IEEE/ASME Trans. Mechatronics*, vol. 18, no. 1, pp. 285–296, Feb. 2013.

[20] O. Y. Chuy, Y. Hirata, Z. Wang, and K. Kosuge, "A control approach based on passive behavior to enhance user interaction," *IEEE Trans. Robot.*, vol. 23, no. 5, pp. 899–908, Oct. 2007.

[21] A. R. Mészáros and K. Shamseddine, "On the solutions of linear ordinary differential equations and Bessel-type special functions on the Levi-Civita field," *J. Contemporary Math. Anal.*, vol. 50, no. 2, pp. 63–42, Mar. 2015.

[22] A. J. Koivo and S. H. Arnautovic, "Control of redundant manipulators with constraints using a reduced order model," *Automatica*, vol. 30, no. 4, pp. 665–677, Apr. 1994.